# Enhancing hydrogen production from steam electrolysis in molten hydroxides via selection of non-precious metal electrodes

Farooq Sher[a,*], Nawar K. Al-Shara[b], Sania Z. Iqbal[c], Zaib Jahan[d], George Z. Chen[b,e,*]

[a] *School of Mechanical, Aerospace and Automotive Engineering, Faculty of Engineering, Environmental and Computing, Coventry University, Coventry CV1 2JH, UK*

[b] *Department of Chemical and Environmental Engineering, University of Nottingham, University Park, Nottingham NG7 2RD, UK*

[c]*Department of Biochemistry, University of Agriculture, Faisalabad 38000, Pakistan*

[d] *School of Chemical and Materials Engineering, National University of Sciences and Technology, Islamabad 44000, Pakistan*

[e] *Department of Chemical and Environmental Engineering, Faculty of Science and Engineering, University of Nottingham Ningbo China, University Park, Ningbo 315100, China*

*Corresponding authors:
E-mail address: Farooq.Sher@coventry.ac.uk (F.Sher), George.Chen@nottingham.ac.uk (G.Chen)

## Abstract

There are still gaps in the field of reference electrode that is needed to assist electrolysis in high temperature electrolytes (e.g. molten hydroxides) for $H_2$ gas production. This research aims to fill the gaps by preparing the $Ni/Ni(OH)_2$ reference electrode and, more importantly, testing its effectiveness against important performance factors, including ion conducting membrane (e.g. mullite tubes), internal electrolyte composition, working temperature and electrochemical control (e.g. potential scan rate). Then, this reference electrode was used to assist the study of the electrocatalytic activity of a range of cheaper working electrode materials, including stainless steel (St.st), Ni, Mo and Ag, in comparison with Pt, by means of chronoamperometry and voltammetry. The effect of introducing steam into the electrolyte (eutectic mixture of NaOH and KOH) on the electrocatalytic activity of each of these working electrodes was also studied. It was observed that

the potential of hydrogen evolution on different working electrodes followed an order of Pt > Ni > St.st > Ag > Mo (positive to negative). The performance of each working electrode was confirmed through chronoamperometry for hydrogen evolution at a constant potential of -0.7 V. It was also found in cyclic voltammetry and confirmed by chronoamperometry that the introduction of steam was apparent in increasing the current density at the cathodic limit for hydrogen evolution. It is hoped that this study will help develop non-precious metal electrodes for the production of the hydrogen fuel. In future, there will be a potential in the threshold concentration of steam for $H_2$ gas production.

# 1  Introduction

An important pollution free fuel that can meet future needs and can also lessen the problems instigated by the consumption of conventional fuels is hydrogen ($H_2$). As a highly efficient fuel, $H_2$ can be used for power generation, transportation and heating, and has the potential to substitute, at least partly, existing fuels. It is well documented and highlighted more recently that the commonly used process for $H_2$ production from water, as a renewable and clean source [1], is electrolysis which splits water into its core ingredients; $H_2$ and oxygen ($O_2$) [2, 3]. Splitting of water, or more accurately steam in high temperature molten hydroxides, by means of electrolysis has great importance and advantages.

52  The main advantage is that in the electrolysis, heat is used as a source of energy and heat is cheaper

53  than electricity in terms of sources and conversion (production). The conductivity of a hydroxide

54  electrolyte at high temperatures is very good and increases with increasing temperature. The

55  hydroxide electrolyte at high temperatures is specific to reduce the loss of energy due to the

56  overpotential of an electrode through acceleration of the reaction kinetics [4]. All these contribute

57  to increasing the net energy efficiency of the process. Molten hydroxides could themselves play

58  the role of a catalyst during the reaction and thus in this technology, there is no need for precious

59  metals as a catalyst [5]. On increasing the temperature, the decomposition voltage of a compound

60  is usually reduced, and this phenomenon is well observed in the case of water electrolysis. In the

61  case of a thermally insulated electrolysis cell, energy consumption is constantly minimised [6].

62  This can be considered for long term electrolysis. Another advantage of electrolysis at high

63  temperatures is that the current flowing continuously through the molten electrolyte contributes to

64  additional internal heating that is needed to compensate any heat loss that is inevitable, even in a

65  thermally well-insulated cell.

66

67  Suitable ion conducting membrane materials are required for the better fabrication of a reference

68  electrode. Therefore, the selection of good ion conducting materials in this field is very important

69  especially in the case of high temperature electrolytes. The redox couple, Ag/AgCl, is commonly

70  used in reference electrodes coupled with different ion conducting membrane materials, such as

71  quartz, Pyrex, porcelain, and mullite [7, 8]. The Ag/AgCl couple contained in silica tube covered

72  with graphite, or enclosed in alumina membrane [9] have also been stated as choices for high

73  temperature molten salts. Selection of membrane materials is important for the fabrication of an

74   electrode in molten hydroxides. Thus, those ionic membranes with good chemical stability,

75   reusability and reproducibility are important [10-12].

76

77   Several studies have previously investigated the use of different working electrodes such as nickel

78   (Ni) [13, 14], platinum (Pt) [15], sliver (Ag) [16] , molybdenum (Mo) [17] or stainless steel (St.st)

79   [18]. These working electrodes have the ability to conduct an adequate catalytic activity for

80   splitting water in hydroxide electrolyte; resulting in the enhancement of reaction kinetics and a

81   subsequent upturn in the production of $H_2$ gas. These metals were either investigated in a molten

82   hydroxide or in an aqueous solution of hydroxide at low temperatures. These studies under

83   different operating conditions used hydroxide and a different type of reference electrode to control

84   the working electrode. For instance, Miles et al. [13] studied the electrochemistry of molten NaOH-

85   KOH salt at 280 $^{o}$C using platinum, nickel and silver as working electrodes against the reference

86   electrode of $Ag^+/Ag$.

87

88   The study of Ge et al. [15] involved cyclic voltammetry on a Pt or Ni wire, or a NiO pellet as the

89   working electrode in fused NaOH at 550 $^{o}$C. A Ni rod was selected as the pseudo reference

90   electrode for the analysis of NiO reduction mechanism into the melt. Zabinski et al. [19] employed

91   a Co-Mo-C alloy to augment the cathodic potential for electrolytic evolution of $H_2$ in a solution of

92   8 M NaOH at 90 $^{o}$C. This was also carried out to inhibit the dissolution of Mo during open circuit

93   dipping in the solution. Another investigation [20] coated the St.st electrode with a Ni-Mo-Fe film

94   to enhance the catalytic activity for $H_2$ evolution in the dilute basic solution. When Ni, Co and

95   NiCo were used as coatings to support a carbon felt electrode, this also resulted in enhanced

96   catalytic activity for the $H_2$ evolution reaction (HER) [21].

97

98    This study is carried out to fabricate and test the $Ni/Ni(OH)_2$ reference electrode with an ion

99    conducting mullite membrane. The reasons behind choosing Ni for the reference electrode

100   fabrication were its range of chemical, physical , electrocatalytic, structural and corrosion resistant

101   properties [22, 23]. Also, the electrocatalytic activity of a range of cheap working electrodes was

102   comprehensively studied against this novel reference electrode. Then, the potentials of these cheap

103   working electrodes for hydrogen gas production via splitting water were assessed in the presence

104   of the eutectic mixture of NaOH-KOH (49:51, mol%) at 300 ºC. The effect of steam at the

105   electrocatalytic activity of these working electrodes has also been studied. Chronoamperometry

106   and cyclic voltammetry were used to investigate the electrocatalytic activity of the working

107   electrodes in this study.

108

## 109   2   Materials and methods

### 110   2.1   The $Ni/Ni(OH)_2$ reference electrode

111   The $Ni/Ni(OH)_2$ reference electrode was fabricated with a mullite tube (Multi-Lab Ltd) as the ionic

112   membrane. The mullite tube consisted of $Al_2O_3$ and $SiO_2$ (36:62, mol%) with the diameter, length

113   and thickness being 5 mm, 500 mm and 1 mm, respectively. The tube had 0.02 vol% of water

114   absorption aptitude with 2.7 g cm$^{-3}$ of bulk density. The internal electrolyte was prepared by mixing

115   1.0 mol% $Ni(OH)_2$ (Arcos Organics) with the eutectic mixture of NaOH and KOH (49:51, mol%).

116   Then this mixture was implanted into the conducting ionic mullite tube. This synthesised mixture

117   was used internally as an electrolyte. The solubility of the $Ni(OH)_2$ in the internal electrolyte of a

118   reference electrode is of great importance. It was described by researchers in past that the

119    dissolution of the $Ni(OH)_2$ in basic solution was not significant at room temperature, this trend was

120    observed to be opposite in case of acidic solution [24].

121

122    On the other hand, $Ni(OH)_2$ has a solubility product of $6.5\times10^{-18}$, and this value was unaffected

123    when noticed from the reaction of $Ni(OH)_2$ with either acid or base. Therefore, a minute amount

124    of 1.0 mol% of $Ni(OH)_2$ was applied in the internal electrolyte. This composition was previously

125    reported for a high $H_2$ evolution rate [25]. The hydroxide mixture (1.16 g) was placed inside the

126    mullite tube which was positioned inside the retort, but it was quickly filled with the mixture of

127    the salts of hydroxides when the tube outside the crucible, to avoid any absorption of moisture

128    contents from the open air. The internal and external composition of the eutectic hydroxides should

129    be the same. The temperature was then raised up to 300 $^oC$ to thoroughly melt the mixtures of

130    hydroxide salts in the mullite tube membrane. The tube was filled up to the length of 12 cm. After

131    that a Ni wire with 0.5 mm diameter and 99.98% pure temper annealed was introduced inside the

132    tube.

133

134    The Ni wire was enclosed inside the mullite tube the left this for overnight to accomplish the

135    melting of the salts mixture at 300 $^oC$. Next to this, the furnace was cooled to the required

136    temperature to solidify the molten melts mixture in the tube and sealed it. Alumina crucible with

137    280 mL volume and 120 mm height (Almath Crucibles Ltd) was used for the performance

138    evaluation of the Ni reference electrode. Argon atmosphere was applied for these test by using an

139    electrochemical analyser of Iviumn Stat multi-channel. For all these experiments 250 g of the

140    molten hydroxides was left in the presence of 40 $cm^3min^{-1}$ of argon gas for 24 h and 300 $^oC$

141    temperature before use. The experimental setup for the designed electrodes is presented in Fig. 1

## 2.2 Specifications of working electrodes

The counter electrode used in this study was prepared of stainless steel rod of 304 Grade, along with the diameter of 5 mm (Unicorn Metals). Five different types of working electrodes were used including Ni, Pt, Ag, Mo, and St.st. The dimensions and properties of these working electrodes are as follows. The 99.98% pure Temper Annealed Ni working electrode was used with a 0.5 mm diameter. The Pt working electrode was 99.95% pure Temper Annealed this was also about 0.5 mm diameter. The third used working electrode was Ag with 99.99% pure Temper Annealed and 1.0 mm in diameter. The Mo working electrode was of 1.0 mm diameter and 99.95% pure Temper Annealed. The last working electrode was St.st with 0.25 mm diameter and 99.99% pure Temper Annealed. All these working electrodes were obtained from Advent Research Material.

The performance of the working electrodes was carried out in a cylindrical alumina crucible using the same protocol as conducted for the reference electrode. Though, it was not easy in practice to attain the exact requisite temperature because the electrolyte temperature is dependant on furnace temperature. So the temperature variation can be controlled by the furnace temperature. The furnace controller of temperature had an accuracy of $\pm 1$ $^{\circ}$C. In addition to the furnace temperature electrolyte temperature was also affected by some other factors. Including the furnace insulation effectiveness and the ambient temperature.

## 2.3 Electrochemical investigation

The electrochemical methods used in this investigation were cyclic voltammetry and chronoamperometry. These techniques were used to study the behaviour of the working electrodes

165 in the molten salts at variable working conditions [26]. The measurements were made between one

166 of the working electrodes (e.g. Ni, Pt, Ag, Mo, St.st) and the designed reference electrode of Ni.

167 The depth of immersion for the working electrodes was ~14 mm inside the electrolyte. Cyclic

168 voltammetry (CV) measurements were noted from negative circuit potential to a positive one.

169 These type of analyses are very important that have already been used in different studies [27, 28].

170 CV investigations were also conducted at different temperatures and in the presence of steam

171 inside molten salts. Introduction of the steam at 7.28 $cm^3$ $min^{-1}$ flow rate was fixed, mixing with

172 argon gas that itself flows at 40 $cm^3$ $min^{-1}$.

173

174 The mixture of argon and steam was effervesced inside the molten salts. CV plots are plotted as

175 current density versus potential. Table 1 shows the working electrodes used in this study, their

176 diameters and calculated surface area respectively. The information regarding the different

177 operating temperatures included as supplementary material. The surface area of the working

178 electrodes can be calculated using Eq. (1).

179

180 $$A = \pi \times D \times h + \frac{1}{4} \times \pi \times D^2 \tag{1}$$

181

182 where A: the surface area of the immersion part inside the melt ($cm^2$), $\pi$: mathematical constant

183 (3.141), D: diameter of the working electrode (cm), and h: the immersion depth of the wire inside

184 the electrolyte (cm).

185

186 ## 3   Results and discussion

187    In this section cyclic voltammetry scans were performed for different working electrodes (e.g. Ni,

188    Pt, Ag, Mo and St.st) in eutectic molten hydroxide as explored below:

189

## 3.1   Cyclic voltammetry investigation of working electrodes

190

### 3.1.1   *Ni working electrode*

191

192    To determine the functioning of different metal electrodes against the designed reference electrode

193    cyclic voltammetry analyses were performed [29, 30]. For this, in the first run blank, Ni wire as a

194    working electrode is used at a temperature of 300 $^o$C and 100 mVs$^{-1}$ scan rate using the prepared

195    nickel reference electrode in molten hydroxide.  Fig. 2(a) displays the obtained cyclic voltammetry

196    full scan.  Fig. 2(b) shows cyclic voltammetry scanned from -0.8 V to -0.1 V vs reference electrode.

197    The latter only focuses on the reduction limit.

198

199    The number of redox peaks can be easily noted as shown in Fig. 2(a).  The C2 peak is the cathodic

200    current credited to the oxide's film reduction [31], made on Ni wire surface, while the A2 peak is

201    anodic current attributed to its oxidation. In addition, the reduction potential started at -0.465V

202    likely corresponds to the evolution of H$_2$ gas [15, 32] and the resultant chemical process is shown

203    in Fig. 2(a) and expressed as reaction (2). The peak A1 is assigned to the generation of oxygen gas

204    as seen in Fig. 2(a) and represented as reaction (3).

205

206    $2\,H_2O + 2e^- \rightarrow H_2(g) + 2\,OH^-$           (2)

207    $2\,OH^- \rightarrow \frac{1}{2}O_2(g) + H_2O + 2\,e^-$           (3)

208    The peak C2 in Fig. 2(a) has a potential of -0.37 V which is scarcely noticeable compared to peak

209    A2 in the first potential cycle (Fig. 2(a)). The redox reactions occurred at the Ni electrode surface

210    in the eutectic molten hydroxides can be credited to this phenomenon [15]. The peak A2 denotes

211    the oxidation of Ni wire [33], which may cause the accumulation of oxide layer on the nickel

212    surface. Consequently, the peak C2 observed because of the reduction of this oxide layer.

213    Furthermore, on limiting the applied voltage between -0.8 V and -0.1 V, the C2 peak vanishes as

214    in Fig. 2(b) due to the lack of oxidation of the nickel wire.

215

216    The disappearance of the reduction peak C2 as shown in Fig. 2(a), reveals that no distinctive

217    reduction peak in this potential scan was confirmed when the scan was limited as shown in Fig.

218    2(b). For the understanding of this reaction, the potential of $H_2O$ and NiO decomposition at 300

219    $^oC$ temperature was measured by the help of HSC 6.0 software. The decomposition reactions are

220    (4 and 5). It reveals from these findings that the two decomposition potentials are quite close,

221    showing that those reactions may occur at the same time during the cathodic sweep. This finding

222    agrees with [15] who stated that the decomposition potentials of water and nickel oxide at 550 $^oC$

223    were very close.

224

225    $H_2O \rightarrow H_2(g) + \frac{1}{2}O_2(g)$   $(E = -1.013 \text{ V})$                                       (4)

226    $2 \text{ NiO} \rightarrow 2 \text{ Ni} + O_2(g)$       $(E = -0.965 \text{ V})$                                       (5)
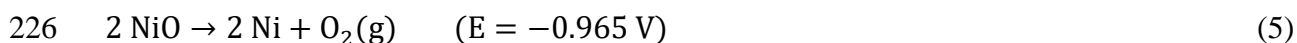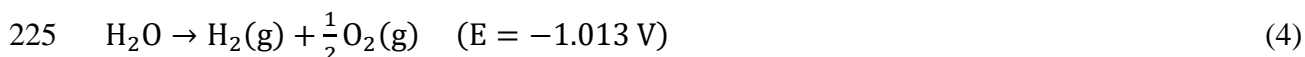
227

228    Fig. 2(c) shows the CV plot of Ni working and reference electrode with and without the presence

229    of steam at a temperature of 300 $^oC$ and 100 mV s$^{-1}$ scan rate. No substantial change in the anodic

230    peak A2 (oxidation of Ni) is witnessed with the introduction of steam inside the molten melt as

231     presented in Fig. 2(c). At cathodic limit, an increase in the current density is noted that increases

232     from -1.6 A cm$^{-2}$ to -2.09 A cm$^{-2}$ with the existence of steam. In order to exhibit the effect of the

233     presence of steam in increasing the evolution of H$_2$ gas, the potential scan is limited between -0.8

234     and -0.3 V as shown in Fig. 2(d). It is obvious from the figure that the reduction potential for the

235     evolution of H$_2$ gas is the same with and without steam. However, the effect of steam can be

236     recognised by enhancing the current density limit for the evolution of hydrogen gas. This increase

237     represents the amount of steam that exists with molten melt and contributed to an increase in the

238     yield of the hydrogen gas.

239

240     ### 3.1.2    *Pt working electrode*

241     In electrochemical studies Pt has great importance because of its good stable characteristics,

242     therefore here Pt working electrode in molten hydroxide is used to achieve reliable CV scans

243     against the designed Ni reference electrode [15]. Fig. 3(a) shows the CV plot of the Pt working

244     electrode in the eutectic molten melt at the same conditions of temperature and scan rate like the

245     previous Ni working electrode. It can be observed from Fig. 3(a) that the anodic limit A1 is

246     observed because of the oxidation of the eutectic molten hydroxides [34] as in reaction (3). While

247     the water reduction, made at the anode, derives the cathodic limit C1 [34]  as in reaction (6).

248

249     $$H_2O + e^- \rightarrow \tfrac{1}{2} H_2(g) + OH^- \tag{6}$$

250

251     Therefore the corresponding potential for hydrogen gas evolution at C2 is  -0.44 V. To focus the

252     scan on the cathodic limit the applied potential is limitised between -0.8 and -0.3 V as shown in

253     Fig. 3(b). As because of this potential limitation, the scan is still stable but the reduction potential

254     shifts negatively to a value of about 0.04 V smaller than the full scan. Furthermore, the potential

255 scan rate varies for the purpose of testation of the platinum working electrode in the settled

256 conditions of temperature and molten hydroxide.

257

258 Furthermore, to the above factors, it is imperative as well to study the effect of steam in the eutectic

259 fused salts with Pt wire working electrode. The reason for investigating this factor is to understand

260 its effect on the behaviour of the platinum working electrode. The cyclic voltammogram scan can

261 translate this change to the behaviour of the electrode. Fig. 3(c) shows the CV scan of platinum as

262 a working electrode with and without the presence of steam. The cyclic voltammetry scan

263 compares the influence of the presences of steam inside the eutectic molten hydroxide with the

264 cyclic voltammetry scan without steam as shown in Fig. 3(c) at a temperature of 300 $^{\circ}$C and a scan

265 rate of 100 mV s$^{-1}$. The presence of steam inside the eutectic molten hydroxide directly affects the

266 obtained cyclic voltammetry scan by increasing the flow of current density at the cathodic limit

267 from 1.16 mA cm$^{-2}$ at C1 to 1.82 mA cm$^{-2}$ at C1'. This attributed to the increase steam bubbles

268 around the cathode which upon electrolysis generate more hydrogen gas this is also well mentioned

269 in literature [35].

270

271 For more clarification, the cyclic voltammetry scans are limited between -0.8 to -0.3 V with and

272 without the presence of steam in the eutectic molten hydroxide, as shown in Fig. 3(d). There is no

273 change in the cyclic voltammetry scan due to this limitation. The presence of steam merely

274 influences the scan by increasing the current density limit of C1 to C1' which represents the

275 reaction of the evolution of hydrogen gas. Even though the platinum electrode is a stable metal in

276 a eutectic molten hydroxide at high temperatures; it still has limited use in the industry because it

277 is classified as a precious metal [36].

12

278

### 3.1.3    Ag working electrode

The blank CV scan is also recorded for a silver working electrode in the studied molten melts, at a 300 °C temperature and 100 mV s$^{-1}$ scan rate as shown in Fig. 4(a). Literature is scarce regarding the exact nature of the silver wire reaction in the hydroxide. For example, the research directed by Miles et al. [13] reported that the reaction of the silver wire in the molten hydroxides may involve $Ag^+\rightarrow Ag$, $AgO_2\rightarrow Ag+O_2$ or some other silver electrode reaction. In this experiment of Ag working electrode with $Ni/Ni(OH)_2$ reference similar findings have been noted as of [13].

A couple of redox peaks observed in the CV scan of Ag electrolysis as displayed in Fig. 4(a). Therefore, the anodic peak A2 may be ascribed to the oxidation whereas the cathodic peak C2 is because of the reduction reaction. These peaks noted because of the oxide layer made on the surface of the silver wire. Moreover, the cathodically augmented current of C1 at -0.52 V corresponds to the evolution of $H_2$ gas, these results are in connection with [32]. Equivalent to this, cathodic chemical reaction shown in equation (2). Reaction (3) represents the generation of oxygen gas as appears in peak A1 of Fig. 4(a). Formation of steam/ or water molecule noted from these mentioned equations.

Subsequently, the cyclic voltammetry scan is limited between -0.8 and -0.3V as shown in Fig. 4(b) to emphasise on the cathodic limit of the evolution of hydrogen gas. It can be observed from Fig. 4(b) that during this limited scanning, there is no considerable change in the starting point of the potential at the cathodic limit. Moreover, it can be noted that the current density at C1' decreased. The current density at the cathodic peak C1 as shown in Fig. 4(a) is roughly about -0.61 A cm$^{-2}$, decreasing to approximately -0.18 A cm$^{-2}$ at C1' Fig. 4(b) during the limited scan potential. The

302  disappearance of the oxidation peak A2 and the reduction peak C2 during the potential scan

303  limitisation is because of the scan starts at potential more negative than the oxidation potential of

304  silver wire. In this case, the decrease in the current density of C1' should be proportional to the

305  silver oxide's reduction to silver. Therefore, it should be mentioned that the silver oxide does not

306  completely reduce at C2, but its reduction is completed at C1 simultaneously with the evolution

307  of hydrogen reaction as seen in Fig. 4(a). This conclusion is based on a noticeable increase in the

308  current density, which otherwise decreases when the potential scan is limited.

309

310  To understand the influence of steam in molten salts on the hydrogen gas evolution with Ag

311  working electrode experiments performed at 300 $^{\circ}$C and 100 mV s$^{-1}$ Fig. 4(d). These experiments

312  were performed on the cathodic limit. The presence of steam with molten melt did not affect the

313  reduction potential of the evolution of hydrogen gas reaction as shown in Fig. 4(d). Thus, the same

314  scan was produced without steam as well. This stable behaviour of the scan can be attributed to

315  how the silver working electrode works in the molten melts against the Ni working electrode. It

316  can also describe in this way that Ag working electrode remains stable and did not show any active

317  response against the steam. Ag stability is somehow opposite to electrocatalytic activity.

318  Moreover, this stable behaviour is associated with the nobel metal properties of the Ag [37, 38].

319  Nobel metals (Ag, Cu and Au) are least reactive against acids that is why use frequently for

320  ornamental purposes due to lower reactivity . So this stable behviour of the Ag metal in steam is

321  directly linked with its noble or inert metal charcteristics, further steam is amphoteric (acts as both

322  acid and base) in nature.

323

324  ***3.1.4   Mo working electrode***

14

325 Molybdenum is one of the transition metals. It has a good electrocatalytic capacity for enhancing

326 the activity of other metals such as nickel [20]. Due to the electroactivity of the molybdenum, it

327 was investigated as a working electrode in this study. Fig. 5(a) and b show the CV of the

328 molybdenum working electrode vs Ni reference electrode at same conditions of temperature and

329 scan rate. It can be observed from Fig. 5(a), that the electrochemical stability window is between

330 A and A' (approximately 0.33 V). The increase in the cathode current density corresponds to the

331 evolution of $H_2$, similar current density increase is detected at C1 and -0.8 V [32]. Equivalent to

332 this, a chemical equation is shown in reaction (2). While anodically an increase in the current at

333 A1 corresponds to the oxygen gas evolution as can be observed in reaction (3).

334

335 The subsequent cyclic voltammetry scan is limited between -0.8 and -0.2V as shown in Fig. 5(b)

336 to focus on the evolution of the hydrogen gas reaction. Therefore, no change in the reduction peak

337 can be noticed if the scan range is limited to the potential located after the potential of the oxidation

338 peak A' reaction takes place. The effect of the presences of steam inside the molten salts on the

339 molybdenum working electrode electrocatalytic behaviour for increasing the hydrogen and oxygen

340 gas evolution is also considered. Fig. 5(c) and Fig. 5(d) show the CV scans of the molybdenum

341 working electrode against the $Ni/Ni(OH)_2$ reference electrode with and without steam with eutectic

342 melt.

343

344 It is obvious from Fig. 5(c) that the effect of the presence of steam is apparent in increasing the

345 current density of the evolution of hydrogen gas at the cathodic limit C1', and the simultaneous

346 evolution of oxygen gas at the anodic limit A1'. At the cathodic limit, the current enhances from -

347 $0.12$ A cm$^{-2}$ without the presence of steam at point C1 to -0.49 A cm$^{-2}$ with the presence of steam

348  at point C1'. At the anodic limit, the current rises from 0.14 A cm$^{-2}$ without the presence of steam

349  at point A1 to 0.465 A cm$^{-2}$ with the presence of steam at point A', these results are in agreement

350  with the literature [39].

351

352  In order to understand the effect of the steam's presence on increasing the current density of the

353  evolution of hydrogen gas reaction, the potential voltammetry scan is limited between -0.8 and -

354  0.3 V respectively as shown in Fig. 5(d). It is very clear from constraining the scan range that

355  there is a considerable effect of the presence of steam in increasing the current density of the

356  evolution of hydrogen gas reaction. It increases from -0.164 Acm$^{-2}$ at C1 to -0.51Acm$^{-2}$ at C1'.

357  This result is shown in Fig. 5(d) through the increase of the molybdenum metal activity with steam

358  and makes a significant change on the H$_2$ evolution.

359

360  ### 3.1.5   St.st working electrode

361  Stainless steel (302) is composed of iron, nickel, chromium, manganese, silicon, carbon,

362  phosphorus and sulphur. It was used in this study as a working electrode to examine its stability

363  and productivity in the molten salts. Fig. 6(a) shows a cyclic voltammetry scan at an operating

364  temperature of 300 $^o$C and a scan rate of 100 mV s$^{-1}$. At the anodic limit A1, the corresponding

365  peak is due to the oxidation of the melt ($2\ OH^- \rightarrow 0.5\ O_2\ (g) + H_2O + 2\ e^-$) while the reduction of

366  the water formed at the anodic limit is seen at the cathodic limit C1. The corresponding reaction

367  of the reduction of water becomes is shown in reaction (6).

368

369  In the case of the oxidation peak A2, it corresponds to the oxidation occurring on the surface of

370  the stainless steel working electrode and the potential of oxidation observed at -0.33 V.

16

371 Subsequently, the CV scan is limited to a range between -0.8 V and -0.3 V in order to focus the

372 scan on the cathodic limit for the HER as shown in Fig. 6(b). No change in the reduction potential

373 which starts at -0.5 V, and the current at the cathodic limit C1 which approximately equals -1.4 A

374 $cm^{-2}$; is discernible. The oxidation peak A2 disappears when the CV scan is limited, even though

375 the potential of the return scan is positive prior to A2 peak.

376

377 Fig. 6(c) and d show the cyclic voltammetry of the stainless steel with and without the presence

378 of steam with molten salts and same working conditions of temperature at 300 $^{o}C$ and scan rate of

379 100 mV $s^{-1}$. No significant change can be observed from the figure regarding the presence of steam

380 with hydroxide salts at the cathodic limit C1 for the evolution of hydrogen reaction as shown in

381 Fig. 6(c). At the oxidation peak, the current density increased from 0.12 A $cm^{-2}$ without the

382 presence of steam (A2') to 0.23 A $cm^{-2}$ with the presence of steam (A2). This increase in the

383 current density from A2' to A2 is responsible for increasing the surface area of the oxide metal.

384

385 The effect of changing the operating temperature of the eutectic molten hydroxide on the working

386 electrode kinetics activity is shown in Fig. S1 was also studied. The studied temperatures were 225

387 and 300 $^{o}C$ respectively. It can be observed that the evolution of hydrogen gas becomes more

388 efficient and sees an increase with increasing temperature for all working electrodes.

389

390 ## 3.2 Working electrode's performance evaluation

391 The stability of the reference electrode in different working conditions and its working comparion

392 against other reference electrode has already been verified in previous studies [30, 40]. The

393 stability, reusability and reproducibility of the Ni/Ni(OH)$_2$ reference electrode have also been

394 reported with good experimentation. This electrode has worked with stability and reproducibility

395    for almost 9 days. Furthermore, a comparison of the reference electrode with other conventional

396    ones ( quasi Pt and Ag)  has also been made.

397

398    After studying the kinetic reaction of each working electrode separately in the eutectic molten

399    hydroxide at different operating conditions respectively; it is imperative to compare their

400    performance. This is essential for discerning which electrode provides more affordable, durable,

401    stable kinetics; and also fast catalytic response for the HER. The comparison focuses mainly on

402    the cathodic limit of the HER. Cyclic voltammetry scans of the different working electrodes (i.e.

403    Ni, Pt, Ag, Mo, St.st) are compared in the eutectic molten hydroxide at a temperature of 300 °C, a

404    potential scan rate of 100 mVs$^{-1}$ and an argon gas atmosphere as shown in Fig.  7.

405

406     It is obvious from Fig.  7 that each working electrode has a unique reduction potential value. It

407    can, therefore, be observed from the above figure that the platinum working electrode had more

408    positive reduction potential value (approximately -0.47 V) followed by the reduction potential of

409    the nickel working electrode (approximately -0.49s V) and then the reduction potential of the

410    stainless steel working electrode at -0.51 V. The reduction potential values of the silver and

411    molybdenum working electrodes occurred at the lower end of the comparison at -0.53 V and -0.56

412    V respectively.

413

414    The results of this study are in close comparison with the literature [41]  in which Ag/AgCl was

415    used as a reference electrode. In this study, current density at the cathodic limit is the highest for

416    nickel working electrode followed by the stainless steel and platinum working electrodes

417    respectively. However, silver and molybdenum have the lowest current density respectively. Table

418    2, displays the reduction potential and the current density at the cathodic limit as observed from

419    the above figure for different working electrodes.

420

421    A high current density measured at the cathodic limit means a high HER. This HER is influenced

422    directly by the electrocatalytic activity of the working electrode inside the eutectic molten

423    hydroxide. As mentioned and tabulated in Table 2. The highest hydrogen evolution reaction that

424    can be achieved at the cathodic limit is done by using the nickel working electrode followed by

425    stainless steel, platinum, silver and finally molybdenum. Therefore, the nickel wire had a higher

426    electrode activity in comparison to the other working electrodes. This behaviour reinforces nickel

427    as a popular choice in electrochemical processes as cathode material for the hydrogen gas evolution

428    reaction. However, some studies such as [42] have revealed that nickel can be deactivated during

429    $H_2$ generation in alkaline water electrolysis and the metal requires the $V_2O_5$ addition to the

430    electrolyte to cause reactivation. These observed results were repeated for three times for all

431    working electrodes, no change on the observed results was experienced.

432

### 3.3  Hydrogen evolution reaction (HER)

434    Fig. 8(a) shows the obtained current-time chronoamperometry at a constant potential of all tested

435    working electrodes in the eutectic molten hydroxide during 10 minutes of the HER. This test was

436    executed at an operating temperature of 300 $^{\circ}$C and 40 $cm^3min^{-1}$ argon atmosphere. The

437    chronoamperograms show that the electrodes change during the first stages of HER, accomplishing

438    a near stationary state. Their reactivity is retained along the noted time period, with platinum

439    followed by nickel being by far, the best one material among the tried (tested) materials and

440    displaying the highest current density values in comparison to stainless steel, silver and

441　molybdenum. This result confirms that the blank metal of platinum and nickel working electrodes

442　in the eutectic molten hydroxide respectively have a better performance for splitting steam to

443　produce hydrogen gas. The stainless steel working electrode is third in order for hydrogen gas

444　production.

445

446　The performance of the different working electrodes was also tested with the presence of steam

447　inside the eutectic molten hydroxide and at an operating temperature of 300 $^{\circ}$C, as shown in Fig.

448　8(b).  It is obvious from the figure that the attained current density value of different working

449　electrodes (without steam) slightly increased with the presence of steam inside the eutectic molten

450　hydroxide. It can also be observed from the above figure that a significant increase in the current

451　density of stainless steel as the working electrode, occurs in the presence of steam. This increase

452　indicates that the electro-catalytic activity of stainless steel under these condition mirrors the value

453　of nickel metal.

454

455　On the other hand, platinum still ranks as the most electro-active for the hydrogen evolution

456　reaction. Despite this, its use was generally limited in history because it is classified as a precious

457　metal in comparison to the others. Similar to steam introduction to increase HER strategy, doping

458　strategy of nanosheets and other conducting materials with heteroatom to increase the

459　electrocatalytic activity and resultantly increase HER, was also applied in literature [43-45] with

460　a positive outcome. In addition to nanosheets, nanocrystals of trimetallic alloy [46]  were also used

461　for HER with high catalytic power. In this study and in other mentioned ones the main focus is the

462　electrocatalytic activity of the materials/ or electrodes which directly plays a key role in HER.

463

# 4  Conclusions

The aims behind this detailed research were to find cheaper, electrocatalytic working electrodes, vs a novel Ni/Ni(OH)$_2$ reference electrode, that can be used to increase the feasibility of hydrogen gas production in eutectic molten hydroxide (NaOH-KOH, 49–51 mol%), at 300 $^o$C temperature. The most important findings that can be drawn from the results are:

- The reduction potential of the hydrogen evolution reaction using different working electrodes was in the order of (more positive to negative reduction potential): Pt > Ni > St.st > Ag > Mo. The performance of each working electrode for the hydrogen evolution reaction was confirmed through chronoamperometry tests at a constant potential of -0.7 V. These tests confirm the stability and productivity of each working electrode. The produced chronoamperograms found that the platinum had the highest current density followed by nickel, stainless steel, silver and then molybdenum at the constant potential of -0.7 V.

- It was also found from the cyclic voltammograms that the presence of steam inside the eutectic molten hydroxide is apparent in increasing the current density at the cathodic limit for the hydrogen evolution reaction. However, the starting point of reduction potential for the hydrogen evolution reaction was still approximately the same with and without the presence of steam inside the eutectic molten hydroxide.

- The effect of increasing the operating temperature of the eutectic molten hydroxide influenced the performed cyclic voltammetry scans. This effect appeared to clearly shift the reduction potential in a positive direction at high temperatures. This positive shift was applicable for all tested working electrodes. The shift in the reduction potential with an increase in the operating temperature was approximately 0.1 V for all tested working

21

486       electrodes. This was despite the fact that each one had a different reduction potential for

487       the hydrogen evolution reaction.

## 488   **Acknowledgement**

# References

1. Yang, J., et al., Achieving excellent dielectric performance in polymer composites with ultralow filler loadings via constructing hollow-structured filler frameworks. Composites Part A: Applied Science and Manufacturing, 2020. 131: p. 105814.
2. Yadav, A. and N. Verma, Efficient hydrogen production using Ni-graphene oxide-dispersed laser-engraved 3D carbon micropillars as electrodes for microbial electrolytic cell. Renewable energy, 2019. 138: p. 628-638.
3. Ganci, F., et al., Nanostructured electrodes for hydrogen production in alkaline electrolyzer. Renewable Energy, 2018. 123: p. 117-124.
4. Hassan, M.H.A., et al., Kinetic and thermodynamic evaluation of effective combined promoters for CO2 hydrate formation. Journal of Natural Gas Science and Engineering, 2020: p. 103313.
5. Licht, S., et al., Comparison of Alternative Molten Electrolytes for Water Splitting to Generate Hydrogen Fuel. Journal of The Electrochemical Society, 2016. 163(10): p. F1162-F1168.
6. Sun, L., et al., Ultrahigh discharge efficiency and improved energy density in rationally designed bilayer polyetherimide–BaTiO 3/P (VDF-HFP) composites. Journal of Materials Chemistry A, 2020. 8(11): p. 5750-5757.
7. Sakamura, Y., Zirconium behavior in molten LiCl-KCl eutectic. Journal of the electrochemical society, 2004. 151(3): p. C187-C193.
8. Gao, P., et al., A quartz sealed Ag/AgCl reference electrode for CaCl2 based molten salts. Journal of Electroanalytical Chemistry, 2005. 579(2): p. 321-328.
9. Wang, H., et al., A robust alumina membrane reference electrode for high temperature molten salts. Journal of The Electrochemical Society, 2012. 159(9): p. H740-H746.
10. Papaderakis, A., et al., Hydrogen evolution at Ir-Ni bimetallic deposits prepared by galvanic replacement. Journal of Electroanalytical Chemistry, 2018. 808: p. 21-27.
11. Abbasi, S., et al., Application of the statistical analysis methodology for photodegradation of methyl orange using a new nanocomposite containing modified TiO2 semiconductor with SnO2. International Journal of Environmental Analytical Chemistry, 2019: p. 1-17.
12. Rashid, T., et al., Formulation of Zeolite-supported Nano-metallic Catalyst and its Application in Textile Effluent Treatment. Journal of Environmental Chemical Engineering, 2020: p. 104023.
13. Miles, M.H., Exploration of Molten Hydroxide Electrochemistry for Thermal Battery Applications. Journal of Applied Electrochemistry, 2003. 33(11): p. 1011-1016.
14. Kadier, A., et al., Hydrogen gas production with an electroformed Ni mesh cathode catalysts in a single-chamber microbial electrolysis cell (MEC). International Journal of Hydrogen Energy, 2015. 40(41): p. 14095-14103.
15. Ge, J., et al., Metallic Nickel Preparation by Electro-Deoxidation in Molten Sodium Hydroxide. Journal of The Electrochemical Society, 2015. 162(9): p. E185-E189.
16. Kacprzak, A., Hydroxide electrolyte direct carbon fuel cells—Technology review. International Journal of Energy Research, 2019. 43(1): p. 65-85.
17. Yavuz, A., et al., Nickel-based materials electrodeposited from a deep eutectic solvent on steel for energy storage devices. Applied Physics A, 2019. 125(8): p. 494.

18.  Ji, D., et al., The optimization of electrolyte composition for CH4 and H2 generation via CO2/H2O co-electrolysis in eutectic molten salts. International Journal of Hydrogen Energy, 2019. 44(11): p. 5082-5089.

19.  Zabinski, P., et al., Electrodeposited Co-Mo-C cathodes for hydrogen evolution in a hot concentrated NaOH solution. Journal of The Electrochemical Society, 2003. 150(10): p. C717-C722.

20.  Jayalakshmi, M., et al., Electrochemical Characterization of Ni-Mo-Fe Composite Film in Alkali Solution. International Journal of Electrochemical Science 2008. 3(8): p. 908-917.

21.  Döner, A., İ. Karcı, and G. Kardaş, Effect of C-felt supported Ni, Co and NiCo catalysts to produce hydrogen. International Journal of Hydrogen Energy, 2012. 37(12): p. 9470-9476.

22.  Al-Shara, N.K., et al., Electrochemical investigation of novel reference electrode Ni/Ni (OH) 2 in comparison with silver and platinum inert quasi-reference electrodes for electrolysis in eutectic molten hydroxide. international journal of hydrogen energy, 2019. 44(50): p. 27224-27236.

23.  Zhou, W.-D., et al., Discriminable Sensing Response Behavior to Homogeneous Gases Based on n-ZnO/p-NiO Composites. Nanomaterials, 2020. 10(4): p. 785.

24.  Gayer, K.H. and A. Garrett, The equilibria of nickel hydroxide, Ni (OH) 2, in solutions of hydrochloric acid and sodium hydroxide at 25. Journal of the American Chemical Society, 1949. 71(9): p. 2973-2975.

25.  Hojamberdiev, M., et al., Synergistic effect of g-C3N4, Ni (OH) 2 and halloysite in nanocomposite photocatalyst on efficient photocatalytic hydrogen generation. Renewable energy, 2019. 138: p. 434-444.

26.  Siwek, K., et al., 3D nickel foams with controlled morphologies for hydrogen evolution reaction in highly alkaline media. International Journal of Hydrogen Energy, 2019. 44(3): p. 1701-1709.

27.  Dastan, D. and A. Banpurkar, Solution processable sol–gel derived titania gate dielectric for organic field effect transistors. Journal of Materials Science: Materials in Electronics, 2017. 28(4): p. 3851-3859.

28.  Dastan, D., et al., Morphological and electrical studies of titania powder and films grown by aqueous solution method. Advanced Science Letters, 2016. 22(4): p. 950-953.

29.  Shan, K., et al., Conductivity and Mixed Conductivity of a Novel Dense Diffusion Barrier and Sensing Properties of Limiting Current Oxygen Sensors. Dalton Transactions, 2020.

30.  Al-Shara, N.K., et al., Electrochemical investigation of novel reference electrode Ni/Ni (OH) 2 in comparison with silver and platinum inert quasi-reference electrodes for electrolysis in eutectic molten hydroxide. International Journal of Hydrogen Energy, 2019.

31.  Zuo, H., et al., Bilayer carbon nanowires/nickel cobalt hydroxides nanostructures for high-performance supercapacitors. Materials Letters, 2020. 263: p. 127217.

32.  Cox, A. and D.J. Fray, Mechanistic investigation into the electrolytic formation of iron from iron (III) oxide in molten sodium hydroxide. Journal of Applied Electrochemistry, 2008. 38(10): p. 1401-1407.

33.  Zhu, X., et al., Fabrication of core-shell structured Ni@ BaTiO3 scaffolds for polymer composites with ultrahigh dielectric constant and low loss. Composites Part A: Applied Science and Manufacturing, 2019. 125: p. 105521.

34.  Híveš, J., et al., Electrochemical Formation of Ferrate (VI) in a Molten NaOH-KOH System. Electrochemistry communications, 2006. 8(11): p. 1737-1740.

579    35.    Al-Shara, N.K., et al., Design and optimization of electrochemical cell potential for
580        hydrogen gas production. Journal of Energy Chemistry, 2020.

581    36.    Couper, A.M., D. Pletcher, and F.C. Walsh, Electrode materials for electrosynthesis.
582        Chemical Reviews, 1990. 90(5): p. 837-865.

583    37.    Diez-Gonzalez, S. and S.P. Nolan, Copper, silver, and gold complexes in hydrosilylation
584        reactions. Accounts of chemical research, 2008. 41(2): p. 349-358.

585    38.    Pierson, J., D. Wiederkehr, and A. Billard, Reactive magnetron sputtering of copper, silver,
586        and gold. Thin Solid Films, 2005. 478(1-2): p. 196-205.

587    39.    Narendranath, J., et al., Electrochemical recovery of hydrogen and elemental sulfur from
588        hydrogen sulfide gas by two-cell system. Energy Sources, Part A: Recovery, Utilization,
589        and Environmental Effects, 2019: p. 1-14.

590    40.    Al-Shara, N.K., et al., Electrochemical study of different membrane materials for the
591        fabrication of stable, reproducible and reusable reference electrode. Journal of Energy
592        Chemistry, 2020.

593    41.    Chaurasia, A.K., H. Goyal, and P. Mondal, Hydrogen gas production with Ni, Ni–Co and
594        Ni–Co–P electrodeposits as potential cathode catalyst by microbial electrolysis cells.
595        International Journal of Hydrogen Energy, 2019.

596    42.    Abouatallah, R., D. Kirk, and J. Graydon, Impedance study of nickel cathode reactivation
597        by vanadium during hydrogen evolution in alkaline water. Electrochemical and solid-state
598        letters, 2002. 5(3): p. E9-E12.

599    43.    Geng, S., et al., Engineering defects and adjusting electronic structure on S doped MoO 2
600        nanosheets toward highly active hydrogen evolution reaction. Nano Research, 2020. 13(1):
601        p. 121-126.

602    44.    Geng, S., W. Yang, and Y.S. Yu, Building MoS2/S-doped g-C3N4 layered heterojunction
603        electrocatalysts for efficient hydrogen evolution reaction. Journal of catalysis, 2019. 375:
604        p. 441-447.

605    45.    Geng, S., et al., Activating the MoS2 Basal Plane by Controllable Fabrication of Pores for
606        an Enhanced Hydrogen Evolution Reaction. Chemistry–A European Journal, 2018. 24(71):
607        p. 19075-19080.

608    46.    Li, M., et al., Modulating the surface segregation of PdCuRu nanocrystals for enhanced
609        all-pH hydrogen evolution electrocatalysis. Journal of Materials Chemistry A, 2019. 7(35):
610        p. 20151-20157.

611

# List of Tables

612

613

| Working electrode | Diameter (cm) | Surface area (cm$^2$) |
|---|---|---|
| Nickel | 0.05 | 0.22 |
| Platinum | 0.05 | 0.22 |
| Silver | 0.10 | 0.44 |
| Molybdenum | 0.10 | 0.44 |
| Stainless steel | 0.025 | 0.11 |

614

615

616

**Table 2.** Reduction potential and the current limit at cathodic limit.

618

| Working electrode | Temperature ($^{o}$C) | Reduction potential $E_{red}$ (V) | Current density $j$ (A cm$^{-2}$) |
|---|---|---|---|
| Ni | 300 | -0.49 | -1.67 |
| Pt | 300 | -0.47 | -1.23 |
| Ag | 300 | -0.53 | -0.20 |
| Mo | 300 | -0.55 | -0.16 |
| St.st | 300 | -0.51 | -1.41 |

619

# Lists of Figures

620

621

622

623



624
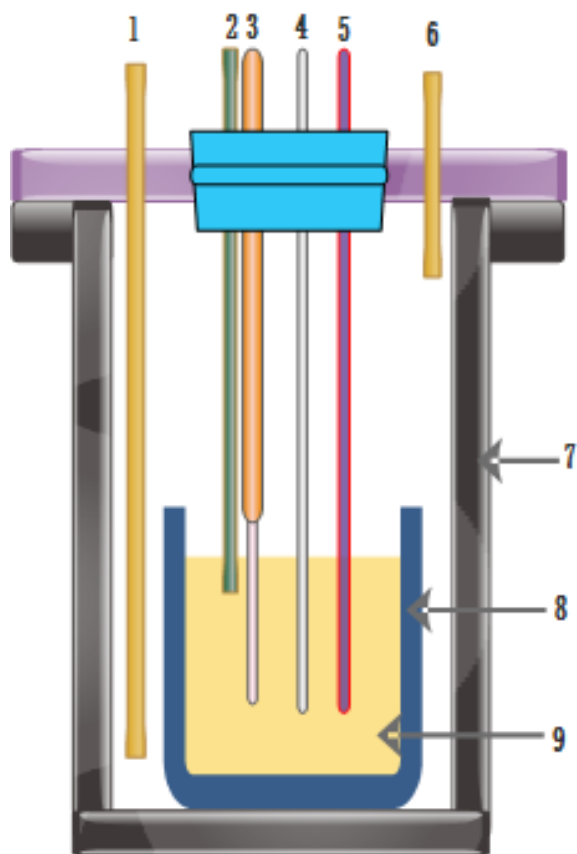
**Fig. 1.** Experimental setup: (1) Argon inlet, (2) Steam inlet, (3) Reference electrode, (4) Working electrode, (5) Counter electrode, (6) Argon outlet, (7), Reaction vessel, (8) Corundum crucible and (9) Molten salt.

627

628



629
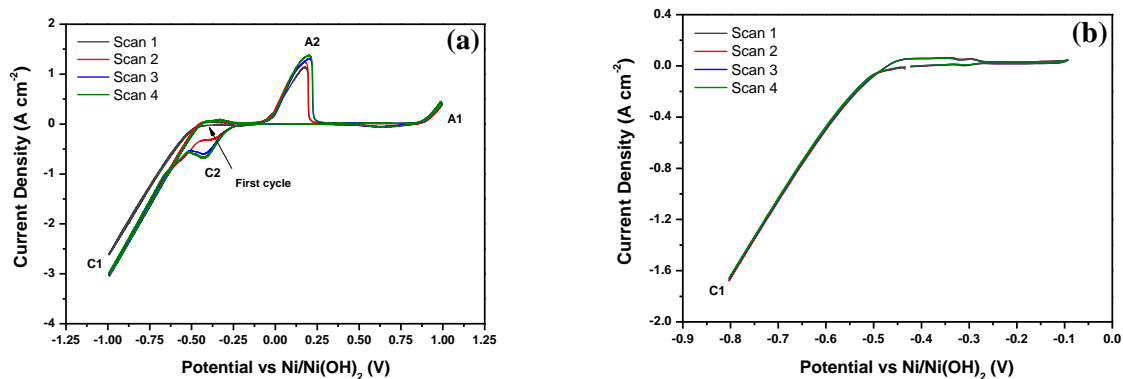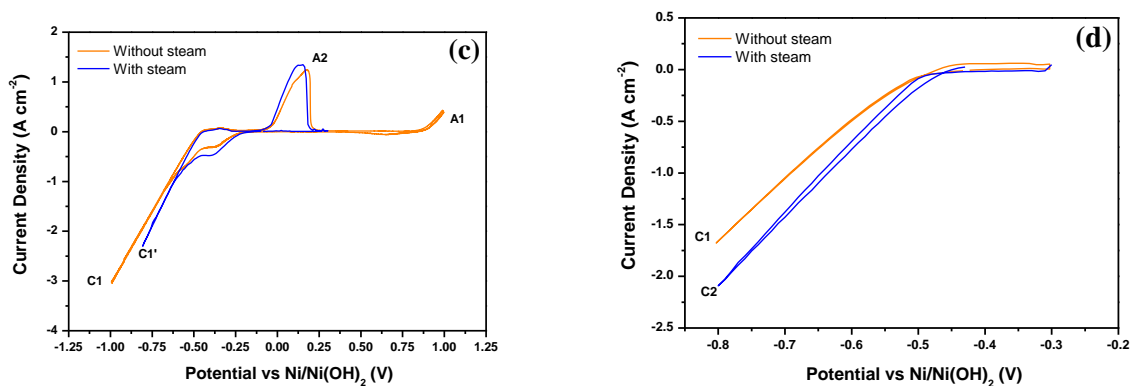
**Fig. 2.** Voltammetric peaks of a 0.5 mm nickel working electrode in the eutectic molten hydroxide at a temperature of 300 °C. RE: Ni/Ni(OH)2; CE: 5 mm stainless steel rod; atmosphere of Ar gas at 40 cm³min⁻¹; the immersion depth : 14 mm; scan rate: 100mVs⁻¹, (a) Scan negatively between -1.0 and 1.0 V, (b) Limiting the scan between -0.8 and -0.1 V, (c) Scan negatively between -0.8 and 1.0 V for steam analysis, (d) Limiting the scan between -0.8 and -0.3 V for steam analysis.

635

636



637
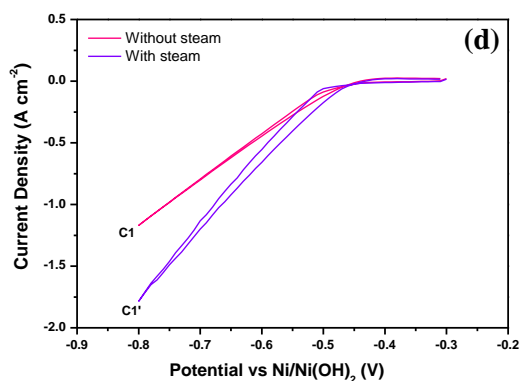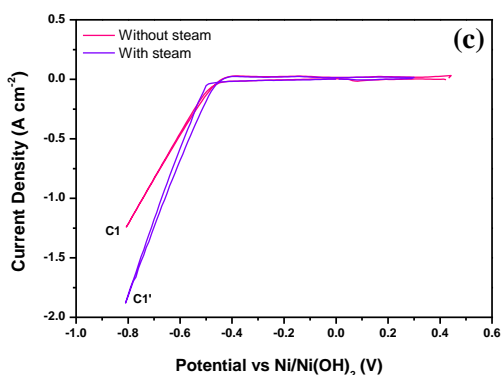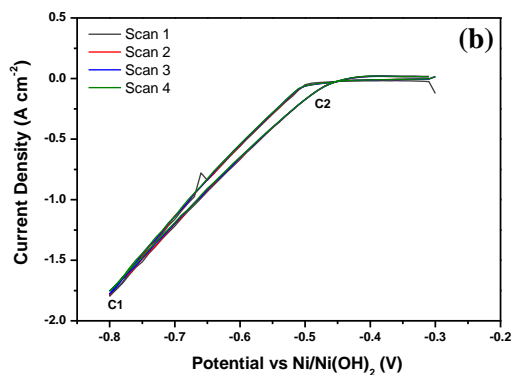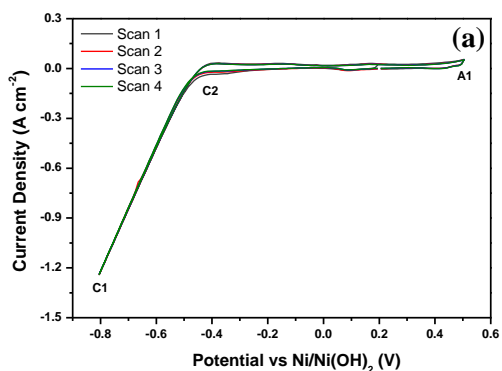


**Fig. 3.** Voltammetric peaks of a 0.5 mm Platinum working electrode in the eutectic molten hydroxide at a temperature of 300 °C. RE: Ni/Ni(OH)$_2$; CE: 5 mm St.st rod; an Ar gas atmosphere at 40 cm$^3$min$^{-1}$; the immersion depth: 14 mm; Scan rate: 100 mV s$^{-1}$, (a) Scan negatively between -0.8 and 0.5 V, (b) ) Limiting the scan between -0.8 and -0.3 V, (c) Scan negatively between -0.8 and 0.5 V for steam analysis, (d) Limiting the scan between -0.8 and -0.3 V for steam analysis.

643

644



645
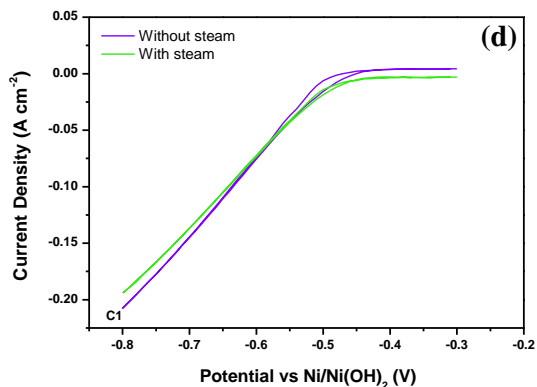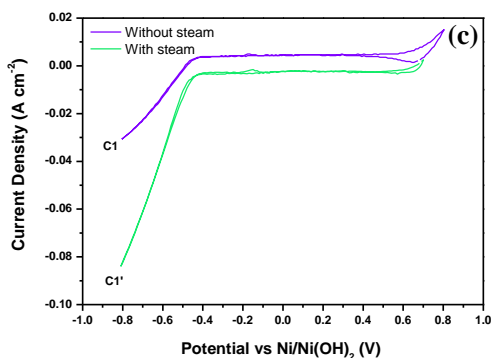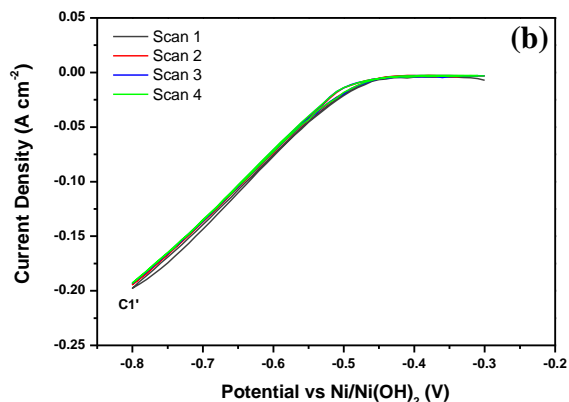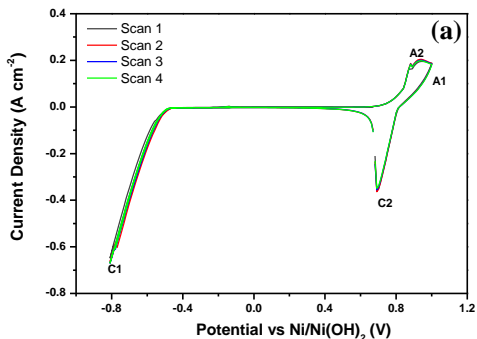


**Fig. 4**. Voltammetric peaks of a 1.0 mm silver working electrode in the eutectic molten hydroxide at scan
rate of 100 mVs$^{-1}$ and operating temperature of 300 $^{\circ}$C. RE: Ni/Ni(OH)$_2$; CE: 5 mm St.st rod; an Ar gas
atmosphere of 40 cm$^3$ min$^{-1}$; the immersion depth: 14 mm; a) Scan negatively from -0.8 to 1.0 V,  (b)
Limiting the scan between -0.8 and -0.3 V, (c) Scan negatively from -0.8 to 1.0 V for steam analysis, (d)
Steam analysis by limiting the scan between -0.8 and -0.3 V.

651

652



653
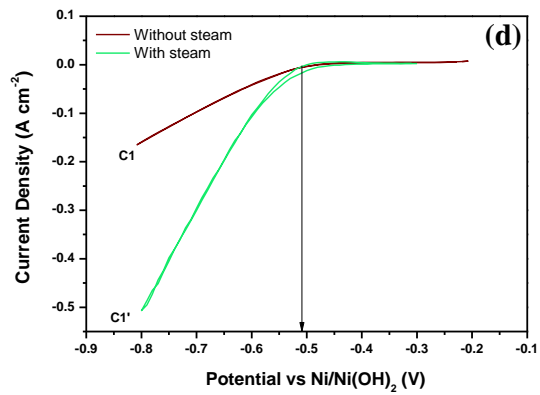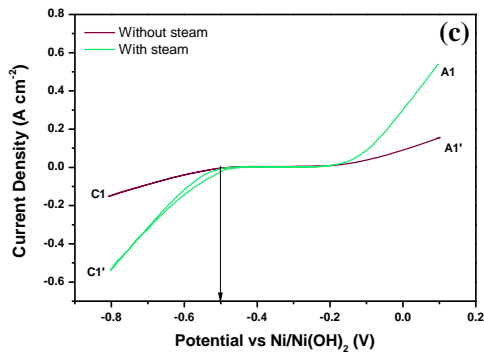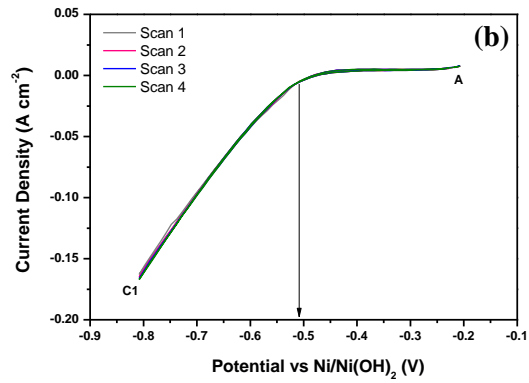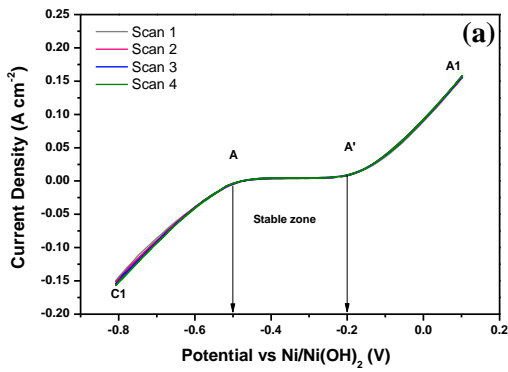


**Fig. 5**. Voltammetric peaks of a 1.0 mm molybdenum working electrode in the eutectic molten hydroxide at a temperature of 300 °C and a scan rate of 100 mV s$^{-1}$. RE: Ni/Ni(OH)$_2$; CE: 5mm St.st rod; an Ar gas atmosphere at 40 cm$^3$min$^{-1}$; the immersion depth: 14 mm; (a) Scan negatively from -0.8 to 0.1V, (b) Limiting the scan between -0.8 and -0.2 V, (c) Scan negatively from -0.8 to 0.1V for steam analysis, (d) Limiting the scan between -0.8 and -0.3 V for steam analysis.

660



661
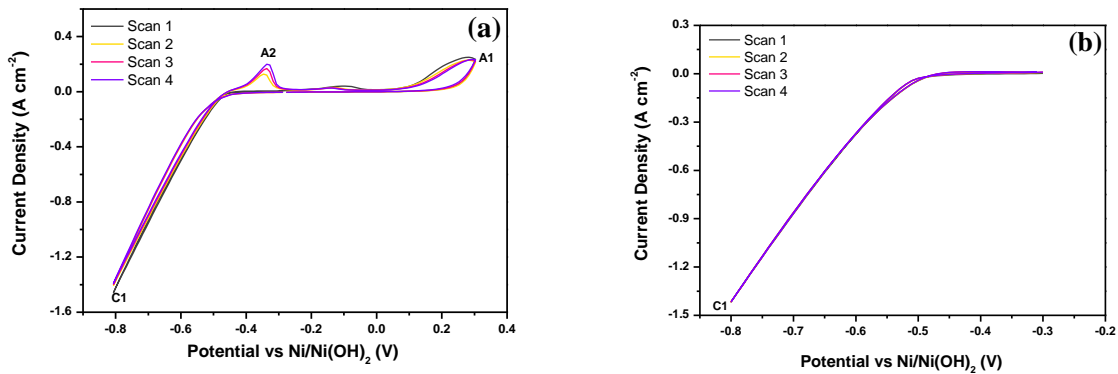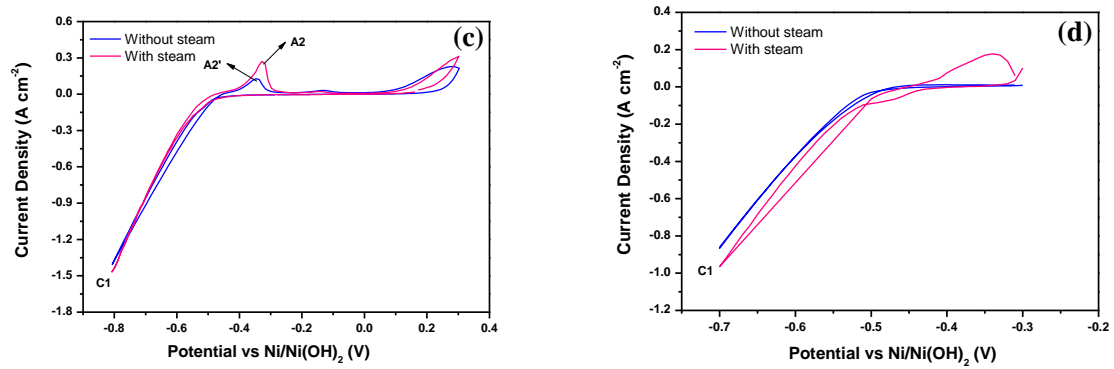
**Fig. 6.** Voltammetric peaks of a 0.25 mm stainless steel working electrode in the eutectic molten hydroxide at a temperature of 300 $^{\circ}$C. RE: Ni/Ni(OH)$_2$; CE: 5 mm St.st rod; an atmosphere of Ar at 40 cm$^3$min$^{-1}$ ; the immersion depth:14mm; Scan rate: 100 mV s$^{-1}$, (a) Scan negatively from -0.8 to 0.3 V, (b) Limiting the scan between -0.8 and -0.3 V (c) Scan negatively from -0.8 to 0.3 V for steam analysis, (d) Steam analysis by limiting the scan between -0.8 and -0.3 V.

668

669

670

671



672
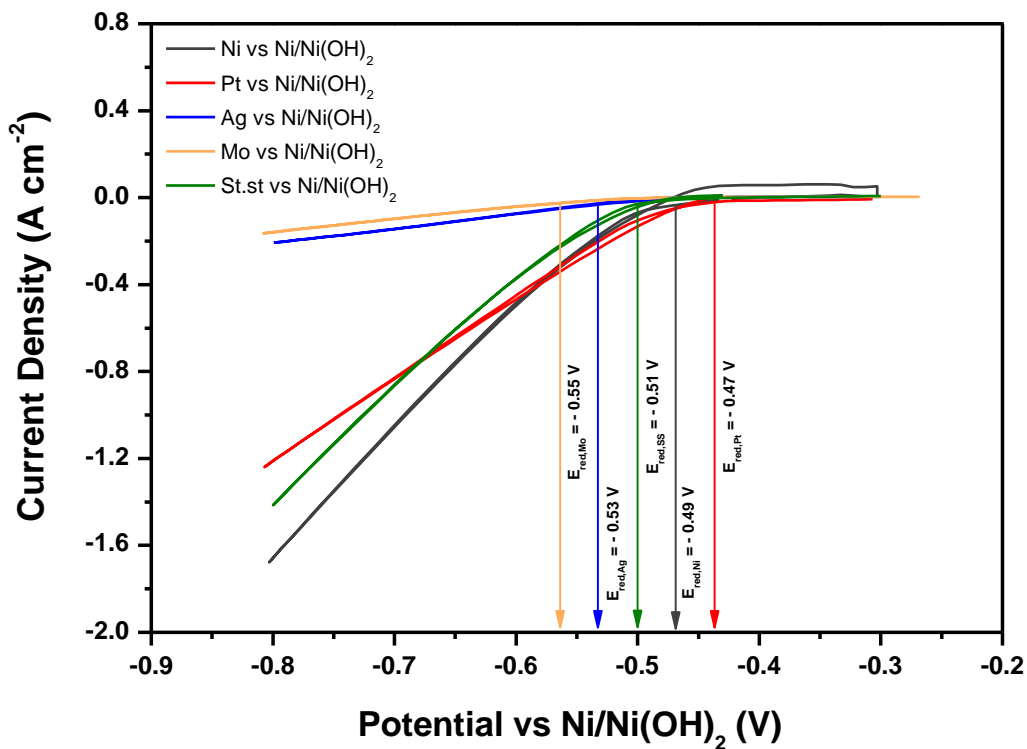
**Fig. 7.** Comparison of cyclic voltammograms of Ni, Pt, Ag, Mo, St.st working electrode in the eutectic molten hydroxide at a temperature of 300 °C and scan rate of 100 mV s⁻¹. RE: 0.5 mm of Ni/Ni(OH)₂ and CE: 5 mm of St.st; immersion depth: 14 mm, an Ar gas atmosphere: 40 cm³min⁻¹.

676
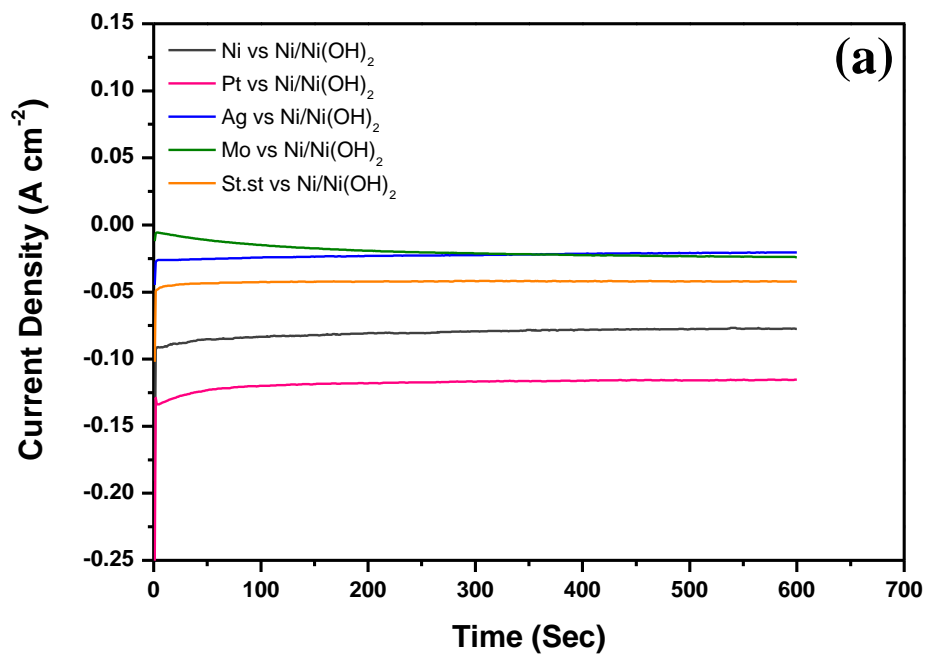
677
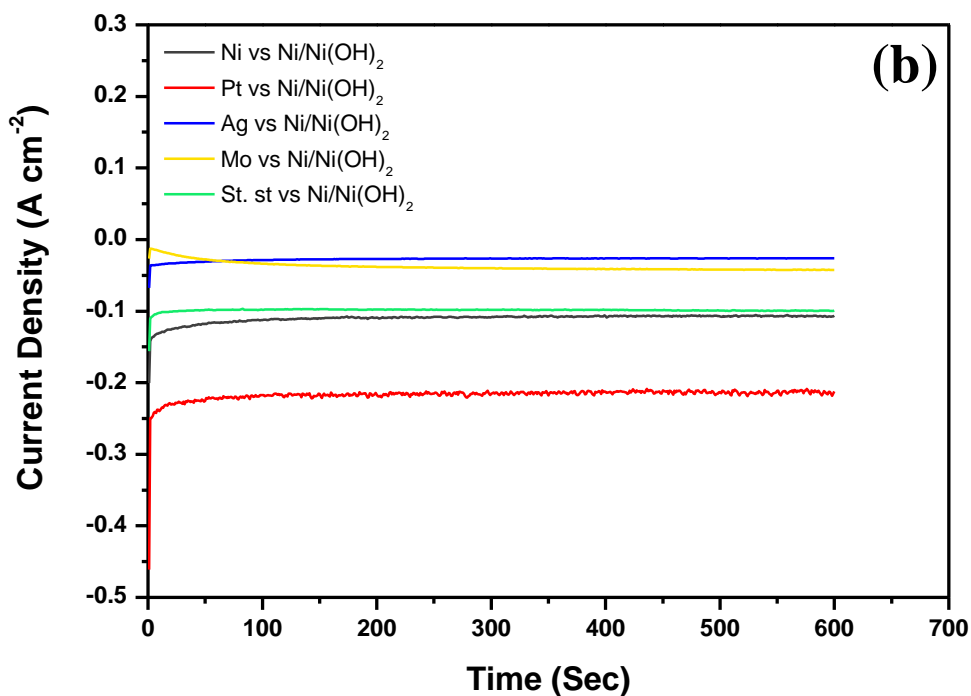


678



679 **Fig. 8.** Chronoamperograms of the hydrogen evolution reaction for all working electrodes (Ni, Pt, Ag, Mo,
680    St.st) in the eutectic molten hydroxide at a temperature of 300 °C, and at an applied potential of -0.7 V

681    during 10 min; (a) Without steam and argon gas atmosphere at 40 $cm^3min^{-1}$, (b) With steam and argon gas
682    atmosphere at 40 $cm^3min^{-1}$.